Journal of Engineering and Applied Sciences 12 (Special Issue 2): 6244-6251, 2017
ISSN: 1816-949X

Design and Analysis of Multi-Input Bidirectional Buck-Boost Converter for Hybrid Electric Vehicles

Mudadla Dhananjaya and Swapnajit Pattnaik
Department of Electrical Engineering, National Institute of Technology,
Raipur, Chhattigarh (CG), India

Abstract: In this study, deals with the design, analysis and control of a multi input, DC/DC converter for the powertrain of a hybrid electric vehicle. The objective is to develop an integral solution of DC/DC converter and control that supports bidirectional operation in order to recover energy during regenerative braking. The presented DC/DC converter topology is a bidirectional buck-boost converter. The stability of this topology is analyzed considering the hybrid electric vehicle application. PI control is the chosen control method for the voltage loop of the bidirectional buck-boost converter due to its robustness and disturbances rejection capability. Then, the voltage PI control is designed by means of the small-signal transfer functions of the multi-input buck-boost converter.

Key words: Multi-input converter, bidirectional operation, small signal, modelling, capability, stability

INTRODUCTION

Concern about global warming is increasing day to day and hence, an alternative requirement of petroleum products has laid the path for the research in utilizing alternative sources of energy for vehicular application. The entire world is highly dependent on transportation system. Most of them use vehicles that have Internal Combustion Engine (ICE). Using the ICE is continuously causing hazardous problems such as global warming, air pollution and the rapid depletion of the Earth's petroleum resources. Electric Vehicles (EV), Hybrid Electric Vehicles (HEV) and Fuel Cell Vehicles (FCV) are the three different vehicles that are proposed to replace conventional vehicles (Kebriaei *et al*., 2015).

These HEV's use alternative energy sources such as wind, PV, battery, fuel cell, ultra-capacitor, etc. (Chan, 2007; Khaligh and Li, 2010; Chan *et al*., 2010). The advantages of HEV's when compared with conventional IC engine vehicles, battery powered fuel cell and EV vehicle is presented by Khaligh and Li (2010). Recent studies have developed a Plug-in-HEV (PHEV) (Gautam *et al*., 2013) which is a hybrid electrical vehicle with rechargeable batteries that can be restored to full charge by connecting the vehicle plug to an external electrical power source.

EV's can be broadly classified into three main categories, viz., hybrid EV's, battery EV's and fuel cell EV's (Gautam *et al*., 2013). An EV should be provided with battery storage for driving the motor or storing energy during regeneration. The battery is generally charged by the electric motor in regeneration mode or from the supply when plugged in. The latter is known to be Plug in EV (PEV) (Soylu, 2011).

According to EPRI report (Rezaee and Farjah, 2014; Rezaee *et al*., 2013) by 2025 the peak share of PHEV's in car market would reach 50% of the whole sale. Tesla Roadster and Nissan Leaf are few to mention. These have a comparable driving specifications like range, speed and low charging time, in addition to their key importance, i.e., zero emission. This proposes much emphasized role of EVs as the key transportation system at least in the cities in the near future.

A power electronic interface unit is essential for matching the voltage levels of the battery and the alternative energy sources used. The function of this converter is to interface different sources with the DC link of DC-AC converter and to control the power flow between the sources (Hintz *et al*., 2015). The performance of vehicle depends on how the power is assigned between the kinds of energy source and how these energy sources are converted to DC bus (Hatami *et al*., 2015). So, DC-DC converters are essential in the system. Each energy source delivers, power to the load through a DC-DC converter in conventional methods which increases the number of devices, size, weight and cost of the multiple number of single input DC-DC converter. Therefore, to overcome the above disadvantages, Multiinput DC-DC Converter (MIC) is used to integrate different sources. Few MIC topologies are reported in literature in which different sources are connected to load through MIC's (Solero *et al*., 2005; Matsuo *et al*., 2004).

Corresponding Author: Mudadla Dhananjaya, Department of Electrical Engineering, National Institute of Technology, Raipur, Chhattigarh (CG), India

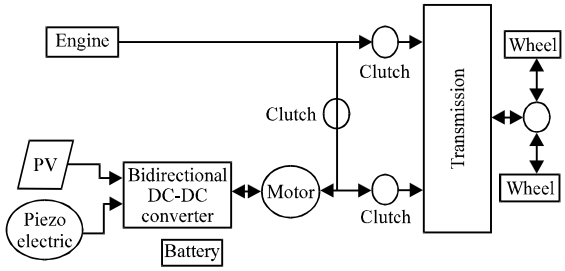

Fig. 1: Schematic diagram of HEV

Using bidirectional non-isolated DC-DC converter improve the operational flexibility of the system (Caricchi *et al*., 1998; Schupbach and Balda, 2003). These have the advantages of fewer components and simple control but cannot provide bidirectional buck-boost power flow capability (Khan *et al*., 2015). Few non isolated bidirectional DC-DC converter were compared and analyzed for PHEV charging applications (Khan *et al*., 2015). Ahmed *et al*. (2013) two bidirectional buck-boost topologies were compared analyzing the pros and cons for electrical vehicle applications.

Liu *et al*. (2010) battery and ultra-capacitor are connected in series using a bidirectional converter and this is in parallel connected to FC supplying the load, this does not provide flexibility to vary voltage across the UC and battery as they are connected across FC directly. Energy flow between multiple source and DC link is presented by Khaligh *et al*. (2009) this uses more number of switches.

There are basically two different hybrid architectures: that can be used for driving the hybrid electric vehicles viz., series and parallel. In series connection of hybrid electric vehicle system the mechanical output from the engine is converted to electrical energy with the help of a generator. This electrical energy is now used, either for charging the battery or to propel the wheels through motor. In parallel connection, ICE and Electric Motor (EM) are used to drive the vehicle. ICE and EM are coupled to drive the shaft of the wheels through two clutches. Depending on the required propulsion power either of ICE or EM or both will drive the vehicle. During regenerative braking the EM acts as generator and charges the battery (Fig. 1).

Photovoltaic system: With the increase in energy demand and depletion in conventional energy sources, the demand for alternative energy sources has been increased over the past few decades. Solar energy in particular has drawn the attention of market and researchers due to the advantages like most abundant in nature, requires less maintenance and environmental friendly. Generally, PV

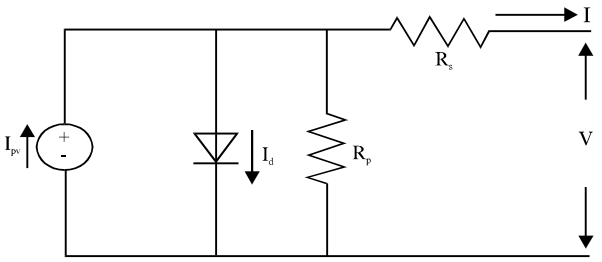

Fig. 2: Equivalent circuit of PV cell

modules composed of a number of PV cells arranged in either parallel (or) series (Ding *et al*., 2012; Villalva *et al*., 2009). Parameters to the PV cell basic (Eq. 1) (Fig. 2):

$$I_{ph} = I_{pv} - I_0\left[\exp\left(\frac{V + R_s I}{A}\right) - 1\right] - \frac{V + IR_s}{R_p} \quad (1)$$

The energy generation of the photovoltaic cell depends on the solar irradiation and it is also influenced by the temperature according to Eq. 2:

$$I_{pv} = \frac{G}{G_n}\left[I_{pv,n} + K_I\left(T - T_n\right)\right] \quad (2)$$

I_0 is the diode saturation current and it is expressed as:

$$I_0 = I_{0,n}\left(\frac{T}{T_n}\right)^3 \exp\left[\frac{qE_g}{Ka}\left(\frac{1}{T_n} - \frac{1}{T}\right)\right] \quad (3)$$

Where:

Eg = The energy of the band gap for Si (Eg = 1.1ev)

I_0, n = The nominal saturation current this will be expressed

$$I_{0,n} = \frac{I_{sc,n}}{\exp\left(\frac{V_{oc,n}}{aV_{t,n}}\right) - 1} \quad (4)$$

Piezoelectric: The number of piezoelectric elements are arranged in a specific manner to generating electrical energy from mechanical energy of a moving a vehicle (or) conventional engine (or) internal combustion engine (Manla *et al*., 2012; Alonso *et al*., 2008). The generated electricity can be stored in the battery and used for moving of the wheel through the power train of traction motor.

MATERIALS AND METHODS

The PZT-5A modules are placed in three strips all along the inner circumference of the tire. The tire chosen has tubes in them. The load experienced by the tire

is profound in the placed in three strips all contact patch area where the modules also experience the mechanical stress. The electrical voltage produced in the modules is fed to the capacitor bank for storage. The modules are arranged as shown in Fig. 3 all around the inner circumference of tire. The modules can be arranged in a single strip or multiple strip (decided according to the contact patch area and tire width). In this calculation, 3 strips the inner circumference of the same is mounted (Makki and Pop-Iliev, 2012; Bai *et al*., 2012).

For calculations of the output voltage certain data indicated in Table 1 is required. The mechanical stress source is basically from the load on the tire which is predominantly the vertical load.

Output power calculations: Since, the vehicle is weighing 250 kg and 50:50 weight, distributed the load on each tire is calculated out to be 125 kg (125×9.81 = 1226.25 N). The modules are to be arranged such that 2 mm gap is maintained between two successive modules. Therefore:

$$\text{No. of modules mounted on each wheel} = \frac{\text{Circumference of the wheel}}{\text{Diameter of each module+gap between two modules}}$$

$$= (\pi \times 457.21)/(28\text{ mm}+2\text{ mm}) = 47$$

Therefore, the total number of modules on each wheel is = 47:

$$\text{The contact patch area} = \frac{\text{Load on the wheel}}{\text{Air pressure in the tire}}$$

$$= (125\times 9.81)/0.1724\text{ N/mm}^2$$

$$= 7112.81\text{ mm}^2$$

Therefore, the contact area almost indulges 3 PZT modules which will be under stress once entering to the contact area zone. Assuming that the load is distributed uniformly in the contact patch area, the mechanical stress induced in each module will be:

$$(\sigma) = \frac{\text{Force on each module}}{\text{Area of application of the load}}$$

$$= (2\times 9.81\times 125)/(3\times \pi \times 0.028^2) = 332079.48\text{ N/m}^2$$

$$\text{Open Circuit Voltage (OCV)} = g_{33}\times \sigma \times t$$

Where:

σ = Induced mechanical stress in the module

t = Thickness of the module

Therefore:

$$O.C.V = 16.6\times 10^{-3}\times 332079.48\times 0.002 = 11\text{ V (approx)}$$

Table 1: Data of the working environment of the system

Parameters	Values
Weight of the vehicle (+2 passengers) (2-wheeler)	250 kg
Weight distribution	50:50
Wheel radius	9" (228.6 mm)
Wheel width	140 mm
Tire air pressure	25 psi
Dimension of PZT-5A module	Diameter 28 mm; Thickness 2 mm
d_{33} (Gautam *et al*., 2013)	350×10-12 C/m^2
g_{33} (Gautam *et al*., 2013)	16.6×10-3 Vm/N

Fig. 3: Mounting of PZT-5A modules

$$\text{Charge Density (CD)} = d_{33}\times \sigma = 350\times 10^{-12}\times 332079.48\text{ N/m}^2 = 0.116227\text{ mC/m}^2$$

Therefore:

$$\text{Charge on each module} = (\text{CD}\times \pi \times \text{width of the contact area}) = 0.0226227\times 3.14\times 0.014^2 = 0.143\ \mu\text{C} = 0.143\ \mu\text{A (for 1 sec)}$$

Thus, the power output = VI = 11×0.143 and μW = 1.573 μW. If the modules in the contact patch area are connected in series then the output voltage of each PZT module just adds up. Therefore, the output voltage now becomes (11×3) V = 33 V and power output is 4.719 μW. For one complete rotation of the wheel the number of times the same power output is obtained is equal to 94. Therefore, the amount of power generated in total = 94×4.719 and μW = 0.434 mW (Approx.).

Assuming the vehicle is running at a speed of 60 kmph, i.e., 16.666 m/sec then the number of wheel rotations per sec is given by:

$$= (\text{Velocity})/(2\times \pi \times \text{radius of the wheel})$$

$$= 16.666/(2\times \pi \times 228.6) = 11.609\text{ rotations/sec}$$

Therefore, power output per wheel per sec = 11.609×0.434 mW = 5.084 mW (approx). If the vehicle runs for 1 h, then the amount of energy that can be stored = $5.084\times 10^{-3}\times 3600 = 18.30$ W. Assuming the similar conditions in all the two wheels, the total amount of energy that can be stored is:

$$= 2\times 18.30\text{ J} = 36.61\text{ W}$$

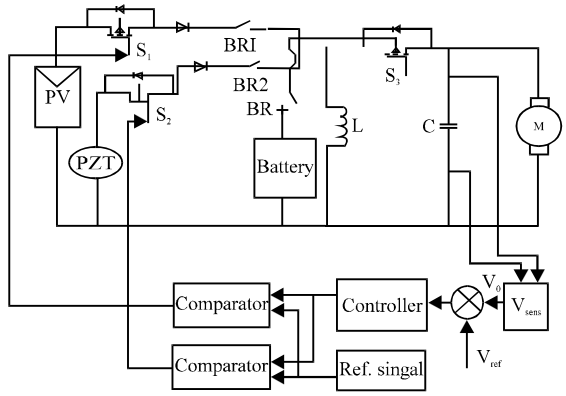

Fig. 4: Schematic of closed loop MBBBC

Circuit topology and operation of multi-input bidirectional buck-boost converter: The Multi-input Bidirectional Buck-Boost Converter (MBBBC) is shown in Fig. 4. With PV, PZT are the input voltage sources. The voltage sources are interfaced through a diode. A common inductance, L has been shared by the energy sources and the output capacitance is C (Bai *et al*., 2012; Sunkara and Kondrath, 2013).

In the presented topology, PV and PZT are the sources selected for driving the motor in HEV. The presented converter operate in two modes. In motoring mode, the sources deliver energy to the motor through the inductor. In case of regenerative mode, the motor feeds energy to the source and is stored in the battery. By the energy stored in the battery can be used with the vehicle for electrical loads in the vehicle. Breakers (BR, BR1, BR2) is connected in series with the battery and sources which are controlled by the load torque of the motor.

Motoring mode

Mode 1 ($0 \le t \le t_1$): In this interval power switch SW_1 is ON, SW_2 is OFF and diode is reverse-biased. The inductor is energized by the input power PV. The inductor current and voltage across capacitor are given by:

$$i_L(t) = \frac{V_{DC1}}{L} t + i_L(0) \quad (5)$$

$$v_C(t) = v_C(0) e^{\frac{-1}{RC} t} \quad (6)$$

Mode 2 ($0 \le t \le t_1$): In the second interval, SW_1 is turned OFF and to avoid the simultaneous conduction of both the switches, SW_2 is not turned ON immediately. By providing delay between the active periods of the two sources avoiding of the converter. The energized inductor transfer its energy to the load. The inductor current and voltage across capacitor in this mode are given by:

$$i_L(t) = e^{-\alpha t}\left[K_1 \cos\omega_d t + K_2 \sin\omega_d t\right] \quad (7)$$

$$v_C(t) = -Le^{-\alpha t}\left[\left(-\alpha K_1 + \omega_d K_2\right)\cos\omega_d t + \left(\omega_d K_1 - \alpha K_2\right)\sin\omega_d t\right] \quad (8)$$

Where:

$$\alpha = \frac{1}{2RC} \quad (9)$$

$$\omega_d = \frac{1}{2}\sqrt{\left(\frac{1}{R^2C^2} - \frac{4}{LC}\right)} \quad (10)$$

$$K_1 = \frac{V_{DC1}}{L} t_1 \frac{e^{\alpha t_1}}{\cos\omega_d t_1}\left[1 - \frac{1}{\omega_d}\left(\omega_d \sin^2\omega_d t_1 + \alpha \cos\omega_d t_1 . \sin\omega_d t_1\right)\right] \quad (11)$$

$$K_2 = \frac{e^{\alpha t_1}}{\omega_d}\frac{V_{DC1}}{L} t_1\left[\omega_d \sin\omega_d t_1 + \alpha \cos\omega_d t_1\right] \quad (12)$$

Mode 3 ($t_2 \le t \le t_3$): In this mode, switch SW_2 is ON, PZT supplies the energy to the inductor and it is energized switch SW_1 and diode are in to OFF state. The inductor current and voltage across capacitor in this mode are expressed as:

$$i_L(t) = \frac{V_{DC2}}{L}\left(t - t_2\right) + e^{-\alpha t_2}\left[K_1 \cos\cos\omega_d t_2 + K_2 \sin\omega_d t_2\right] \quad (13)$$

$$v_c(t) = -e^{\frac{-1}{RC}(t - t_2)} L\left[e^{-\alpha t_2}\begin{bmatrix}\left(-\alpha K_1 + \omega_d K_2\right)\cos\omega_d t_2 + \\ \left(\omega_d K_1 - \alpha K_2\right)\sin\omega_d t_2\end{bmatrix}\right] \quad (14)$$

Mode 4 ($t_3 \le t \le t_4$): In this interval power switches SW_1, SW_2 are OFF, diode will be forward-biased through load and capacitor is charged reversely by the demagnetization of inductor (L). The inductor current and voltage across capacitor in this mode are expressed as:

$$i_L(t) = e^{-\alpha t}\left[K_3 \cos\omega_d t + K_4 \sin\omega_d t\right] \quad (15)$$

$$v_C(t) = -Le^{-\alpha t}\left[\left(-\alpha K_3 + \omega_d K_4\right)\cos\omega_d t + \left(\omega_d K_3 - \alpha K_2\right)\sin\omega_d t\right] \quad (16)$$

Where:

$$K_3 = \frac{V_{DC2}}{L}\left(t_3 - t_2\right) + \frac{1}{\cos\omega_d t_3}\left[K_1 \cos\omega_d t_2 + K_2 \sin\omega_d t_2\right] - K_4 \tan\omega_d t_3 \quad (17)$$

$$K_4=\frac{e^{\alpha t_3}}{\omega_d}\left[\begin{array}{l} e^{\frac{-1}{RC}(t_3-t_2)}\left[e^{-\alpha t_2}\left[\begin{array}{l}(-K_1+{}_dK_2)\cos{}_dt_2+\\ (\omega_dK_1-\alpha K_2)\sin\omega_dt_2\end{array}\right]\right]+\\ (1+\alpha)\left[\frac{V_{DC2}}{L}(t_3-t_2)+e^{-\alpha t_3}\left[K_1\cos\omega_dt_2+K_2\sin\omega_dt_2\right]\right]\end{array}\right] \quad (18)$$

Small signal modelling of DC-DC converter: Small signal analysis of the power converter is concerned with modelling of the averaged, linearized, small signal AC behavior around a state operating point of the system. The information obtained from this investigation can be used to predict the system transfer function that is useful in the feedback loop design. The small signal analysis and state-space equation of capacitor voltage and inductor current of the converter for different modes of operation is performed (Ramanarayanan, 2008):

$$A=\begin{bmatrix}0 & -\left[1-(d_1+d_2)\right]/L\\ 1-(d_1+d_2)/C & -1/RC\end{bmatrix} \quad (19)$$

$$B=\begin{bmatrix}V_0+V_{in}/L\\ -I_0/C\end{bmatrix} \quad (20)$$

$$C=\begin{bmatrix}0 & 1\\ d_1+d_2 & 0\end{bmatrix} \quad (21)$$

$$D=0 \quad (22)$$

$$\hat{x}=\begin{bmatrix}\hat{i}_L\\ \hat{v}_C\end{bmatrix}\hat{u}=\begin{bmatrix}\hat{d}_1\\ \hat{d}_2\end{bmatrix} \quad (23)$$

$$G(s)=C(SI-A)^{-1}B+D \quad (24)$$

$$=\frac{(V_0+V_{in})\left[1-(d_1+d_2)\right]}{LC}-\frac{I_0S}{C}\Big/S\left(S+\frac{1}{RC}\right)+\frac{\left(1-[d_1+d_2]\right)^2}{LC} \quad (25)$$

$\hat{i}_L, \hat{v}_C, \hat{d}_1, \hat{d}_2$ are perturbations of i_L, v_C d_1 and d_2, respectively.

Controller modelling and stability analysis: The open loop system consists of two complex conjugate poles on imaginary axis which drives the response of G(s) into marginally stable, i.e., system response becomes oscillatory. To reduce the undamped behavior and to guarantee the stability of the closed loop system a controller ([Gc(s)] and compensator [Gcom(s)]) is cascaded with MBBBC (G(s)). The implementation of PI controller will improve the low frequency performance, i.e., it reduces the steady state error. Also a compensator is cascaded with PI controller to improve transient performance. The pole placement technique have been used for better design of the parameters for the controller to obtain the desired step response (Narasimharaju *et al*., 2010). The generalized transfer function of PI controller is given by Fig. 5:

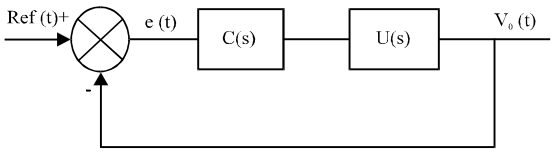

Fig. 5: Design of closed loop controller for converter voltage

$$G_c(s)=K_P+\frac{K_I}{s} \quad (26)$$

Equation 34 can be written as:

$$G_c(s)=\left(\frac{K_Ps+K_I}{s}\right) \quad (27)$$

Transfer function of lead-lag compensator is:

$$G_{com}(s)=\left(\frac{s+a}{s+b}\right) \quad (28)$$

where, a and b are zero and pole, respectively. From Eq. 27 and 28:

$$C(s)=G_c(s)\times G_{com}(s) \quad (29)$$

$$=\left(\frac{s+a}{s+b}\right)\left(\frac{K_Ps+K_I}{s}\right) \quad (30)$$

$$C(s)=\frac{K_P(s+a)^2}{\left(s^2+sb\right)} \quad (31)$$

$$G_{cl}(s)=\frac{C(s)G(s)}{1+C(s)G(s)} \quad (32)$$

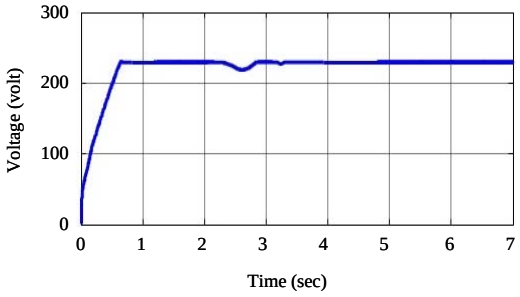

Fig. 6: Converter output voltage

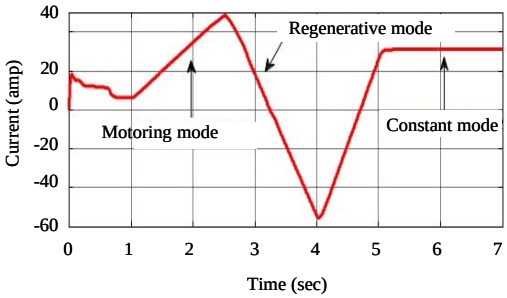

Fig. 7: Motor speed

RESULTS AND DISCUSSION

Simulation results: For analyzing the different modes of operation to different load torques are set at different time intervals from 0-1 sec load torque is set at 5 N/m. And started varying from 5-50 N/m in the time interval 1-2.5 sec at 2.5 sec the load torque is 50 N/m and hence, a small transient is observed in the output voltage of the converter at 2.5 sec but due to the controller action the transient last for very small period and reaches the reference value as shown in Fig. 6. Due to change in load torque from 5-50 N/m the motor speed decreases and motor current increases. In the time interval 1-2.5 sec as shown in Fig. 7 and 8. As varied from 50-60 N/m in the time interval 2.5-4 sec to check regenerative mode of operation it was observed that the speed has been increased in the time interval due to decrease in the load torque as shown in Fig. 7 due to negative load torque the current flows from source to load as observed in Fig. 8 this negative current will flow into the battery, charging it. In Fig. 10, it is observed that SOC of the battery is indicating charging of the battery in regenerative mode. The load torque increased from -60 to 30 N/m in the time interval 4-5 sec there by again operating the motor in motoring mode and load torque is kept constant at 30 N/m form 5-7 sec the corresponding changes in the speed and current can be observed in Fig. 7 and 8, respectively. Changes in the load torque with respect to time explained is shown in Fig. 9, the frequency response of MIBBBC system with controller is analyzed through bode plot the

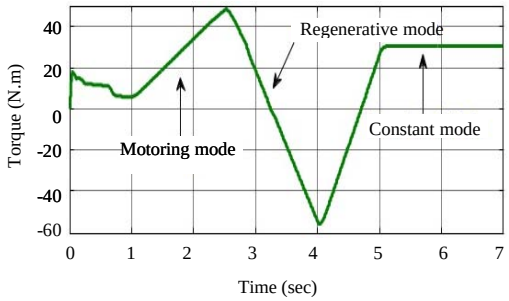

Fig. 8: Motor current

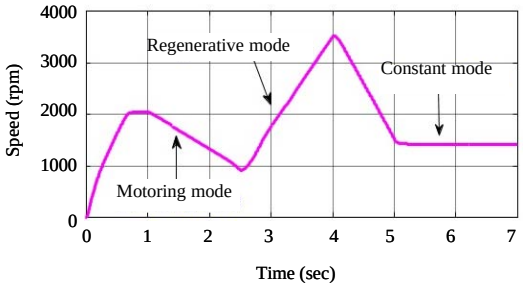

Fig. 9: Motor torque

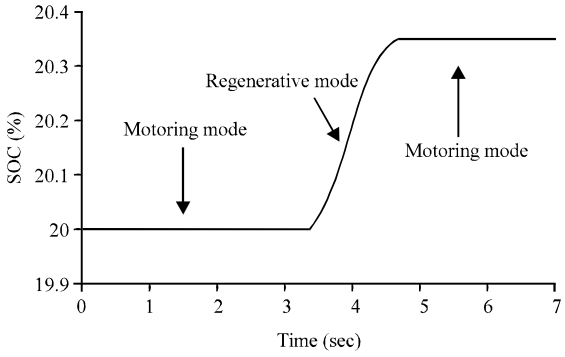

Fig. 10: Battery SOC

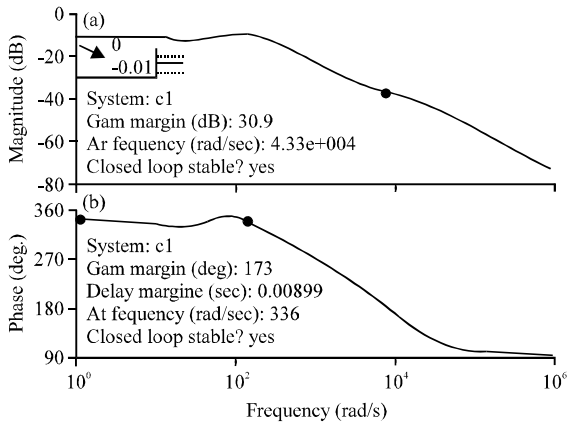

Fig. 11: Bode plot of the system with controller

system with controller is analyzed through bode plot the gain margin and phase margin are 30.9 dB and 173°, respectively obtained from the magnitude and phase plot which confirms stability of the system shown in Fig. 11.

CONCLUSION

In this study, the design, analysis, control and implementation of a multi input bidirectional DC/DC converter for an HEV powertrain are proposed, The development of this solution comprises the design and analysis of the chosen buck-boost converter topology, the design and implementation of a PI control for this converter, the addition of a PI control to regulate the output voltage. PI control has been proven to be a robust technique in front of system uncertainties. In this case, it is shown that regenerative operation is allowed with no need to change the control method and not even determining whether the converter is operating in step-up or step-down mode.

REFERENCES

Ahmed, A., M.A. Khan, M. Badawy, Y. Sozer and I. Husain, 2013. Performance analysis of bi-directional dc-dc converters for electric vehicles and charging infrastructure. Proceedings of the 2013 IEEE Conference on Energy Conversion Congress and Exposition (ECCE), September 15-19, 2013, IEEE, Denver, Colorado, ISBN:978-1-4799-0337-5, pp: 1401-1408.

Alonso, J.M., C. Ordiz and M.A.D. Costa, 2008. A novel control method for piezoelectric-transformer based power supplies assuring zero-voltage-switching operation. IEEE. Trans. Ind. Electron., 55: 1085-1089.

Bai, S., Q. Xu, L. Gu, F. Ma and Y. Qin et al., 2012. Single crystalline lead zirconate titanate (PZT) nano/micro-wire based self-powered UV sensor. Nano Energy, 1: 789-795.

Caricchi, F., F. Crescimbini, F.G. Capponi and L. Solero, 1998. Study of bidirectional buck-boost converter topologies for application in electrical vehicle motor drives. Proceedings of the 13th Annual IEEE Conference on Applied Power Electronics and Exposition (APEE 1998) Vol. 1, February 15-19, 1998, IEEE, Anaheim, California, ISBN:0-7803-4340-9, pp: 287-293.

Chan, C.C., 2007. The state of the art of electric, hybrid and fuel cell vehicles. Proc. IEEE., 95: 704-718.

Chan, C.C., A. Bouscayrol and K. Chen, 2010. Electric, hybrid and fuel-cell vehicles: Architectures and modeling. IEEE. Trans. Veh. Technol., 59: 589-598.

Ding, K., X. Bian, H. Liu and T. Peng, 2012. A MATLAB-simulink-based PV module model and its application under conditions of nonuniform irradiance. Energy Convers. IEEE. Trans., 27: 864-872.

Gautam, D.S., F. Musavi, W. Eberle and W.G. Dunford, 2013. A zero-voltage switching full-bridge DC-DC converter with capacitive output filter for plug-in hybrid electric vehicle battery charging. IEEE. Trans. Power Electron., 28: 5728-5735.

Hatami, A., M.R. Tousi, P. Bayat and P. Bayat, 2015. Power management strategy for hybrid vehicle using a three-port bidirectional DC-DC converter. Proceedings of the 23rd Iranian Conference on Electrical Engineering (ICEE) 2015, May 10-14, 2015, IEEE, Tehran, Iran, ISBN:978-1-4799-1973-4, pp: 1498-1503.

Hintz, A., U.R. Prasanna and K. Rajashekara, 2015. Novel modular multiple-input bidirectional DC-DC Power Converter (MIPC) for HEV/FCV application. IEEE. Trans. Ind. Electron., 62: 3163-3172.

Kebriaei, M., A.H. Niasar and B. Asaei, 2015. Hybrid electric vehicles: An overview. Proceedings of the 2015 International Conference on Connected Vehicles and Expo (ICCVE), October 19-23, 2015, IEEE, Shenzhen, China, ISBN:978-1-5090-0264-1, pp: 299-305.

Khaligh, A. and Z. Li, 2010. Battery, ultracapacitor, fuel cell and hybrid energy storage systems for electric, hybrid electric, fuel cell and plug-in hybrid electric vehicles: State of the art. IEEE. Trans. Veh. Technol., 59: 2806-2814.

Khaligh, A., J. Cao and Y.J. Lee, 2009. A multiple-input DC-DC converter topology. IEEE. Trans. Power Electron., 24: 862-868.

Khan, M.A., A. Ahmed, I. Husain, Y. Sozer and M. Badawy, 2015. Performance analysis of bidirectional DC-DC converters for electric vehicles. IEEE. Trans. Ind. Appl., 51: 3442-3452.

Liu, W.S., J.F. Chen, T.J. Liang, R.L. Lin and C.H. Liu, 2010. Analysis, design, and control of bidirectional cascoded configuration for a fuel cell hybrid power system. IEEE. Trans. Power Electron., 25: 1565-1575.

Makki, N. and R. Pop-Iliev, 2012. Battery-and wire-less Tire Pressure Measurement Systems (TPMS) sensor. Microsyst. Technol., 18: 1201-1212.

Manla, G., N.M. White and M.J. Tudor, 2012. Numerical model of a non-contact piezoelectric energy harvester for rotating objects. IEEE. Sens. J., 12: 1785-1793.

Matsuo, H., W. Lin, F. Kurokawa, T. Shigemizu and N. Watanabe, 2004. Characteristics of the multiple-input DC-DC converter. IEEE. Trans. Ind. Electron., 51: 625-631.

Narasimharaju, B.L., S.P. Dubey and S.P. Singh, 2010. Coupled inductor bidirectional DC-DC converter for improved performance. Proceedings of the 2010 International Conference on Industrial Electronics, Control & Robotics (IECR), December 27-29, 2010, IEEE, Orissa, India, ISBN:978-1-4244-8544-4, pp: 28-33.

Ramanarayanan, V., 2008. Course Material on Switched Mode Power Conversion. Indian Institute of Science, Bengaluru, India, Pages: 460.

Rezaee, S. and E. Farjah, 2014. A DC-DC multiport module for integrating plug-in electric vehicles in a parking lot: Topology and operation. IEEE. Trans. Power Electron., 29: 5688-5695.

Rezaee, S., E. Farjah and B. Khorramdel, 2013. Probabilistic analysis of plugin electric vehicles impact on electrical grid through homes and parking lots. IEEE. Trans. Sustainable Energy, 4: 1024-1033.

Schupbach, R.M. and J.C. Balda, 2003. Comparing DC-DC converters for power management in hybrid electric vehicles. Proceedings of the IEEE International Conference on Electric Machines and Drives (IEMDC03) Vol. 3, June 1-4, 2003, IEEE, Madison, Wisconsin, ISBN:0-7803-7817-2, pp: 1369-1374.

Solero, L., A. Lidozzi and J.A. Pomilio, 2005. Design of multiple-input power converter for hybrid vehicles. IEEE. Trans. Power Electron., 20: 1007-1016.

Soylu, S., 2011. Electric Vehicles the Benefits and Barriers. Intech Open Access Publisher, Rijeka, Croatia, ISBN:978-953-307-287-6, Pages: 252.

Sunkara, S. and N. Kondrath, 2013. Design and Pspice simulation of synchronous bidirectional PWM DC-DC buck-boost converter operating in CCM. Proceedings of the 2013 Annual IEEE Conference on India (INDICON), December 13-15, 2013, IEEE, Mumbai, India, ISBN:978-1-4799-2276-5, pp: 1-6.

Villalva, M.G., J.R. Gazoli and E.R. Filho, 2009. Comprehensive approach to modeling and simulation of photovoltaic arrays. IEEE Trans. Power Electron., 24: 1198-1208.